Supplementary information

Anchor active sulfur/selenium into enhanced carbon hosts with multiple chemical affinity for efficient K-S/Se batteries

Yongxu Du,*[a] Hongguang Fan,[b] Yujing Zhu,[a] Xianghua Zhang,[a] Denghu Wei,[a] Chuanyu Jin, [a] Yongpeng Cui [c] and Meiying Lv*[a]

[a]School of Materials Science and Engineering, Liaocheng University, Liaocheng 252000, China

[b]School of Materials Science and Engineering, Qingdao University of Science and Technology, Qingdao 266061, China

*Corresponding author.

E-mail address: duyongxu@lcu.edu.cn (Y. Du)

E-mail address: lvmeiying@lcu.edu.cn (M. Lv)

1. Experimental Section

1.1 Material Synthesis.

The MSTC hollow carbon was prepared by previous work. [1] Then, the MSTC and commercial selenium power or sulfur powder were mixed with a mass ratio of 2:3 by using a mortar and pestle. The mixtures were sealed and heated in a tube furnace at 166 °C (S) and 266 °C (Se) for 12 h under an Ar atmosphere to ensure the melt-diffusion S or Se into the nanopores of MSTC, respectively. The obtained samples are named as MSTC@S and MSTC@Se. The comparative samples were prepared by the same method without heat, which are named MSTC mixed S and MSTC mixed Se.

1.2 Materials characterizations

The morphological characteristics of various samples were investigated by SEM (Hitachi S4800) and TEM (JEM-2100). The crystalline phase of the as-prepared samples was characterized by XRD analysis (Bruker AXS, Germany) using Cu Kα radiation. The Raman spectra were obtained on a JobinYvon HR800 Raman spectrometer with a 532 nm. X-ray photoelectron spectroscopy (XPS) tests were obtained on a Thermo ESCALAB 250 XI spectrometer using a monochromatic Al-Ka X-ray source. The nitrogen adsorption-desorption isotherms were obtained using a Micromeritics 3 Flex™ surface characterization analyzer at 77K. The specific surface area of various samples was calculated by the BET method, while the pore size distributions were determined by the BJH method. Thermogravimetric (TG) analysis tests were performed on a TG/DSC 2HT 1600 instrument (Mettler-Toledo, Germany). The electrical conductivity of varoius samples was test on four-probe resistance tester tester (ROOKO, FT-340).

1.3 Electrochemical Measurements

The corresponding electrochemical performance of samples was tested by assembling CR2032 type cion cells assembled in an Ar-filled glove box. The electrodes consisted of 80 wt.% active materials, 10 wt.% acetylene black and 10 wt.% PVDF binder was prepared by coating a slurry with a designated thickness on the collector followed by drying in a vacuum oven overnight at 80 °C for 12 h. The areal S or Se loading in the K-S or K-Se cell electrode is about 1.5 mg cm^{-2}, respectively. For K-S or K-Se batteries, potassium foils were used as both the reference and counter electrode. 1 M potassium bis(fluorosulfonyl)imide (KFSI) dissolved in an ethylene carbonate (EC) - diethyl carbonate (DEC) (1:1 v/v) was used as electrolyte and glass fibers (Whatman, GF/D) was used as the separator. Galvanostatic charge and discharge cycling, rate capability tests, and galvanostatic intermittent titration technique (GITT) were carried out with a Land battery measurement system (CT2001A) between 0.5 and 3 V versus K/K^+. For GITT tests, the cell was measured at a pulse current of 50 mA g^{-1} for 30 min, followed by a relaxation period of 120 min. Cyclic voltammetry (CV) and electrochemical

impedance spectroscopy (EIS) were tested on the Gamry 1010E electrochemical analyzer (Warminster, PA, USA). All electrochemical tests were carried out at room temperature and the capacities were calculated based on the weight of the S or Se in the active materials.

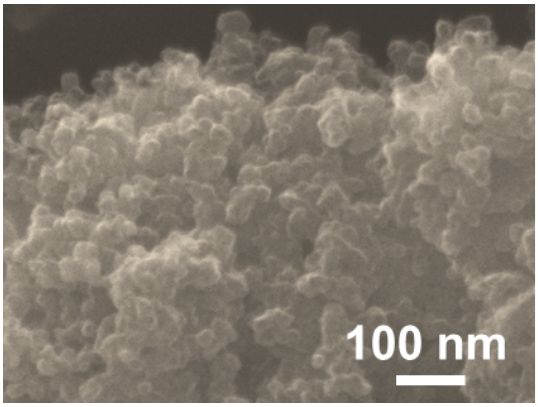

Figure S1.The SEM image of MSTC

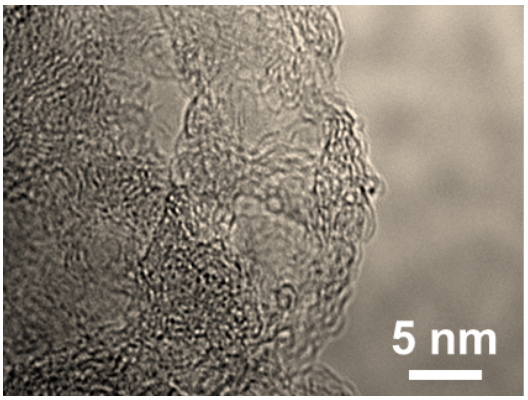

Figure S2.The TEM image of MSTC

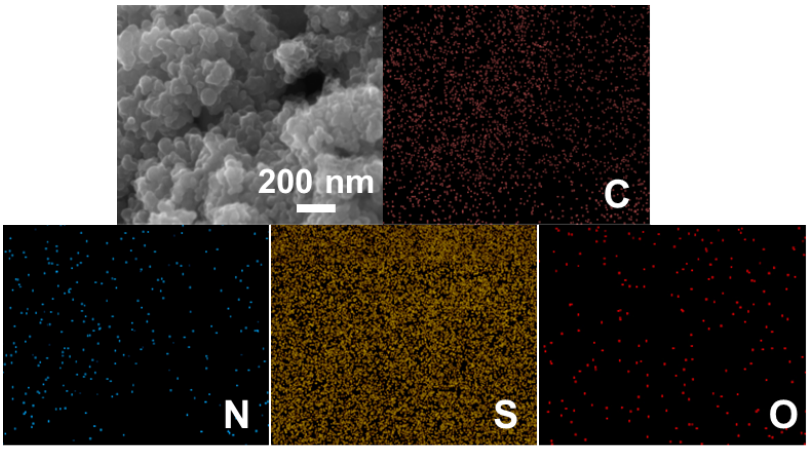

Figure S3. The SEM image and corresponding EDS mapping of MSTC@S.

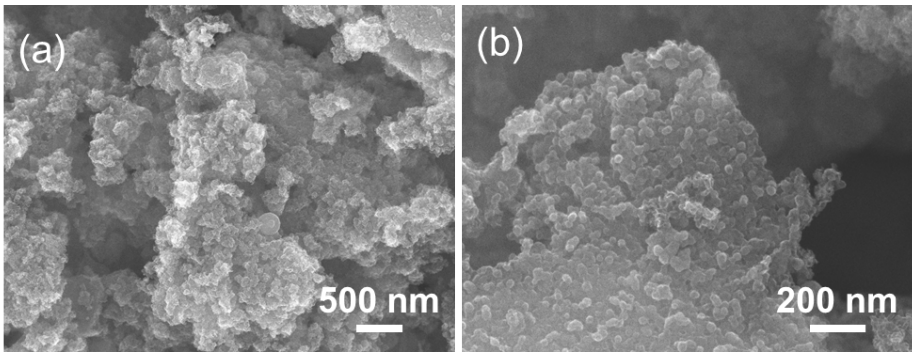

Figure S4. (a, b) The SEM images of MSTC mixed with S powder.

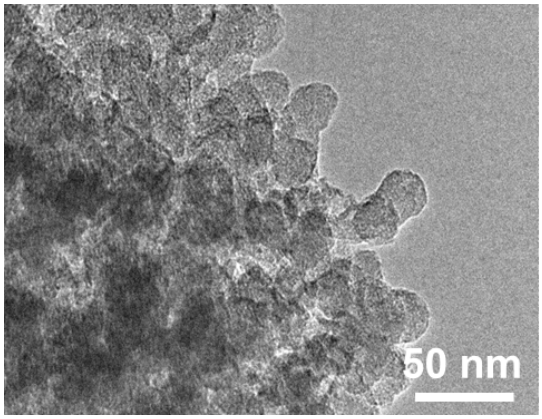

Figure S5. The TEM image of MSTC@S.

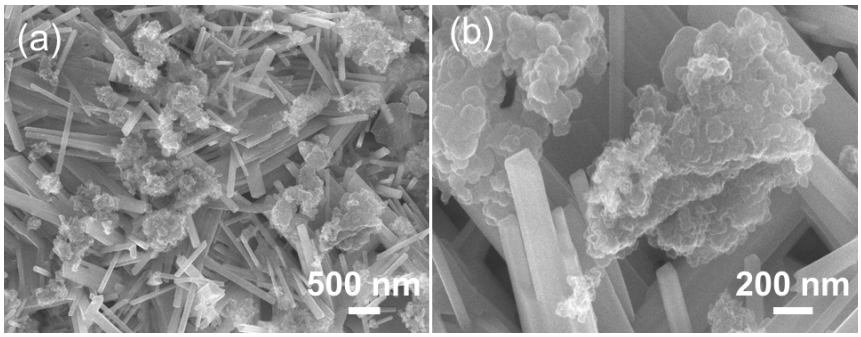

Figure S6. (a, b) The SEM images of MSTC mixed with Se powder.

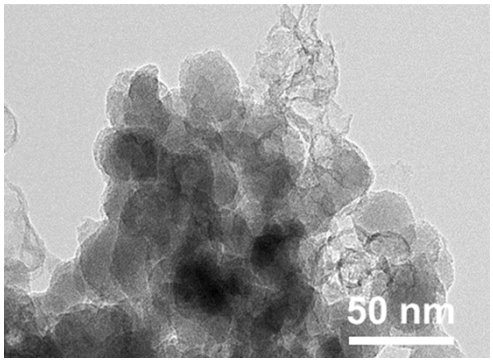

Figure S7. The TEM image of MSTC@Se.

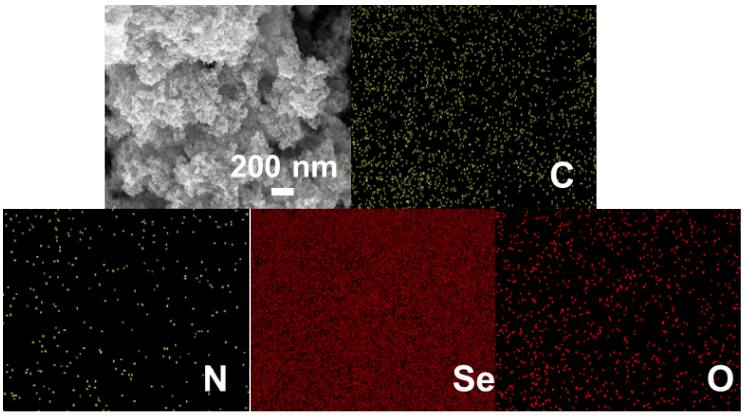

Figure S8. The SEM image and corresponding EDS mapping of MSTC@Se.

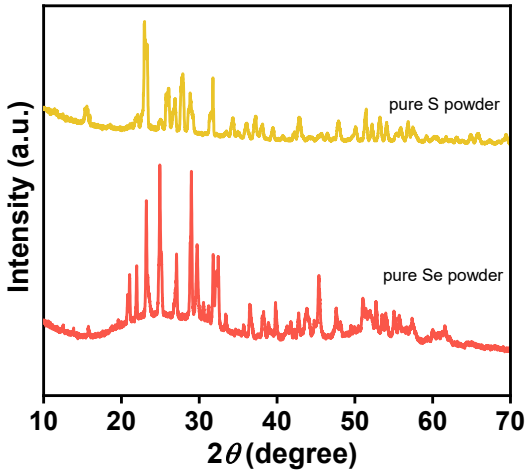

Figure S9. XRD patterns of pure S and Se powder.

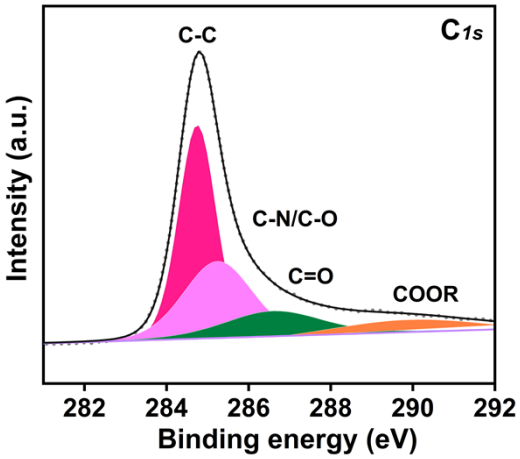

Figure S10. High-resolution XPS spectra C*1s* of MSTC.

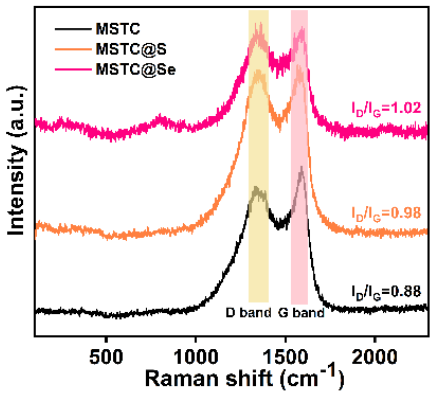

Figure S11. Raman spectra of MSTC, MSTC@S and MSTC@Se.

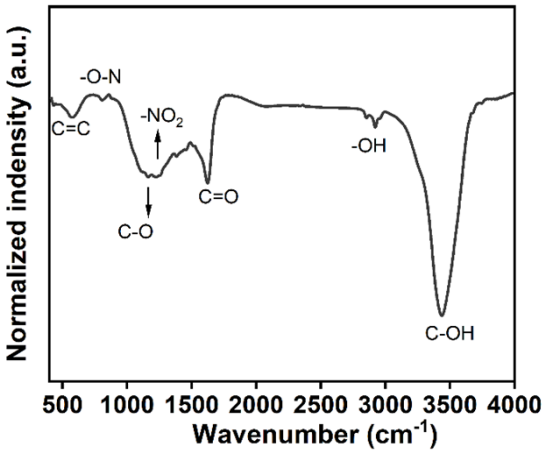

Figure S12. FT-IR spectra of MSTC.

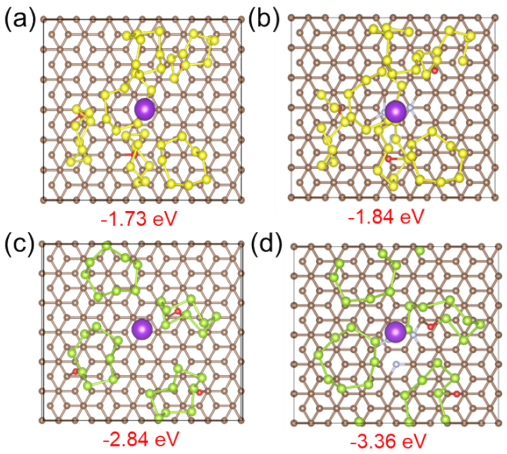

Figure S13. Different functional group types and corresponding models of the optimal sites of a single K atom adsorbed in the (a) MSTC@S only with O, (b) MSTC@S with O and N, (c) MSTC@Se only with O, and (d) MSTC@Se with O and N.

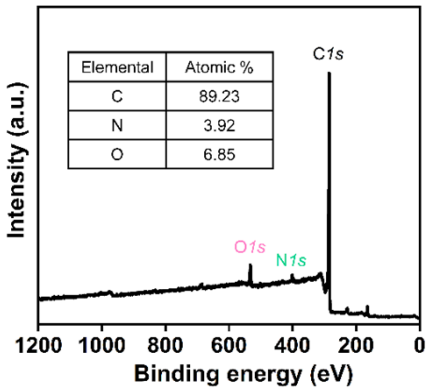

Figure S14. The XPS spectrum of MSTC.

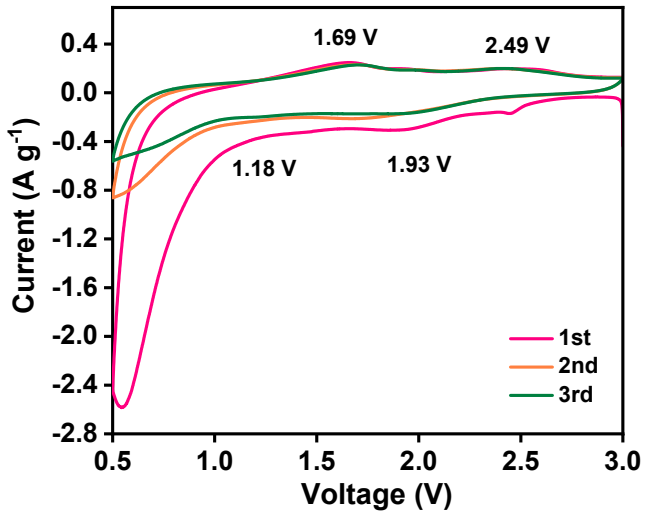

Figure S15. CV curves of first three cycles of MSTC@S cathode at 0.2 mV s^{-1}.

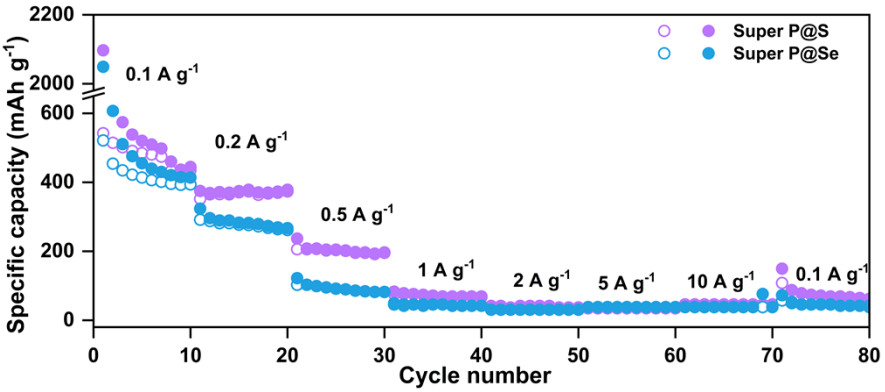

Figure S16. The rate capability of Super P@S and Super P@Se at different current densities.

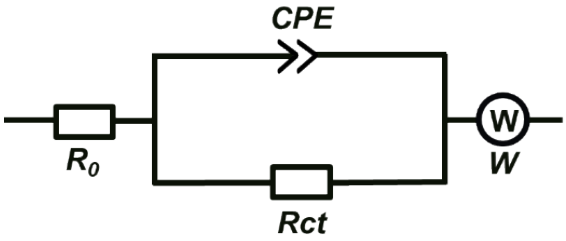

Figure S17. The corresponding equivalent circuit.

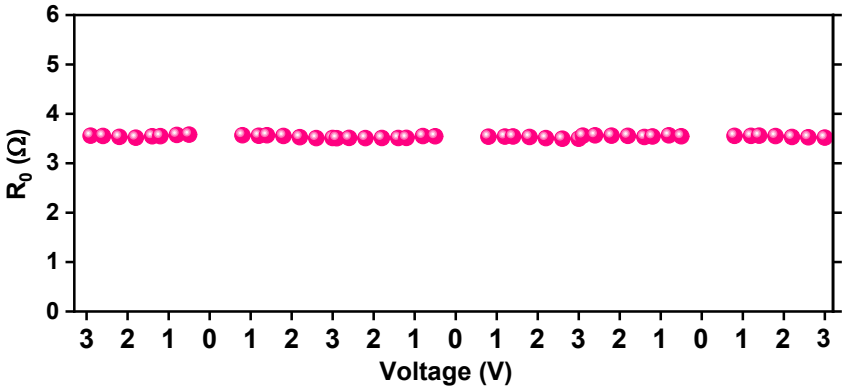

Figure S18. The intrinsic ohmic resistance (R_0) of MSTC@Se.

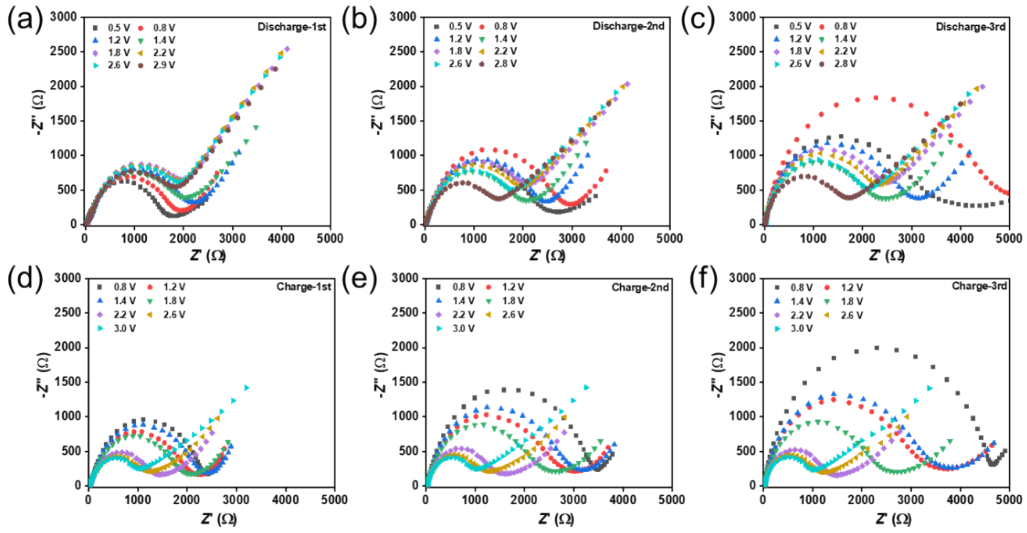

Figure S19. (a-f) Nyquist plots of MSTC@Se at different potentials during first three discharge/charge processes.

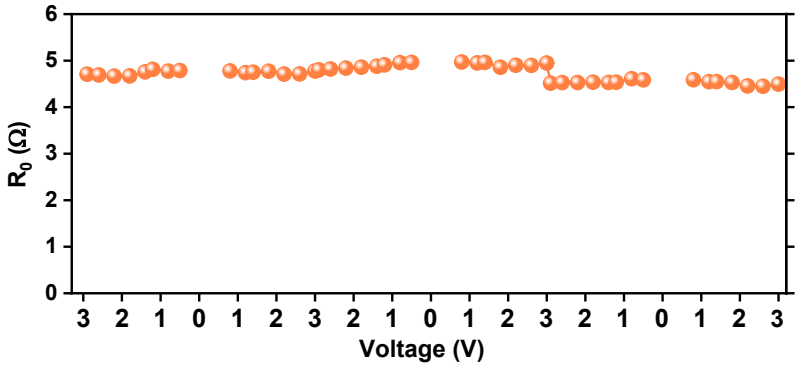

Figure S20. The intrinsic ohmic resistance (R_0) of MSTC@S.

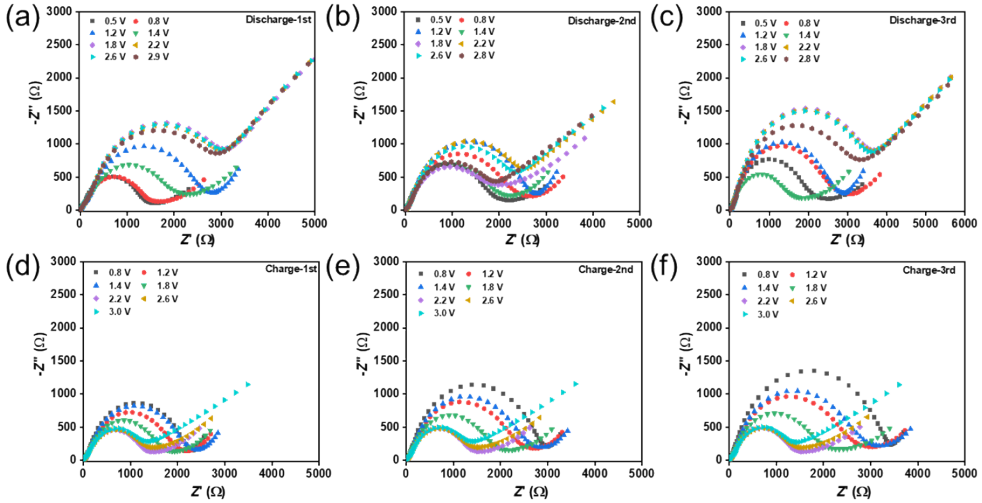

Figure S21. (a-f) Nyquist plots of MSTC@S at different potentials during first three discharge/charge processes.

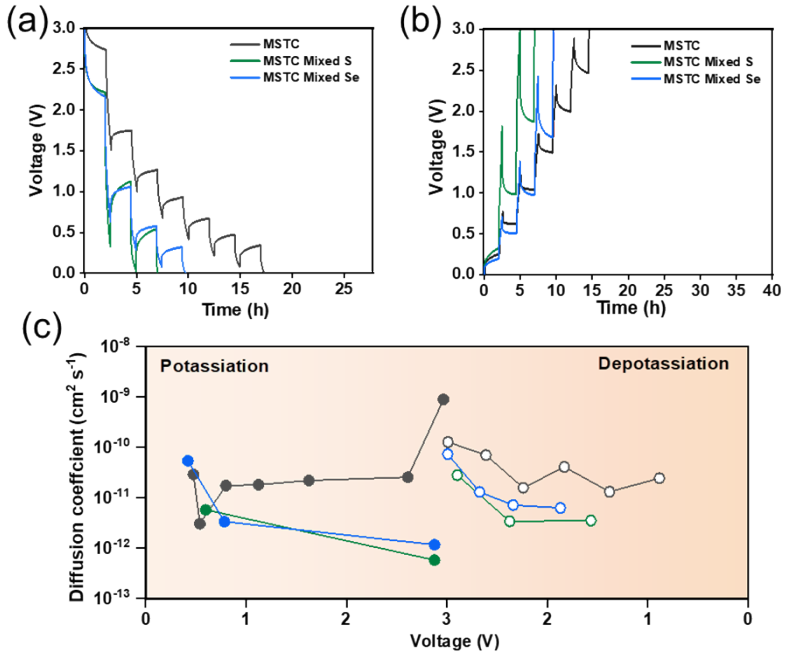

Figure S22. (a, b)GITT curves and (c) the corresponding D_{K+} of various samples at discharge state and charge state.

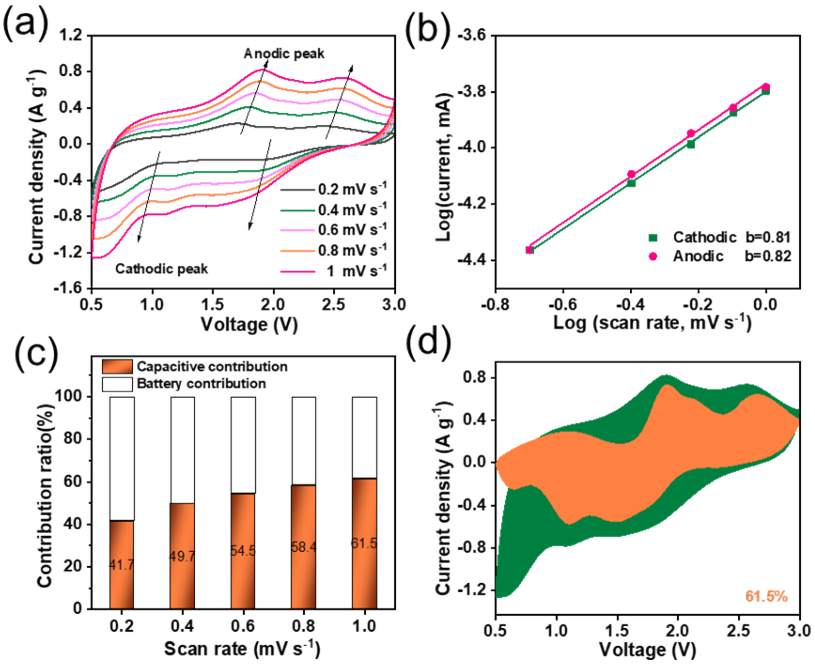

Figure S23. (a) CV curves at different scan rates, (b) determination of the *b*-value according to the relationship between peak current and scan rate, (c) normalized contribution proportions of capacitance and diffusion at different scan rates, and (d) capacitive contribution at 1 mV s^{-1} of the MSTC@S electrode.

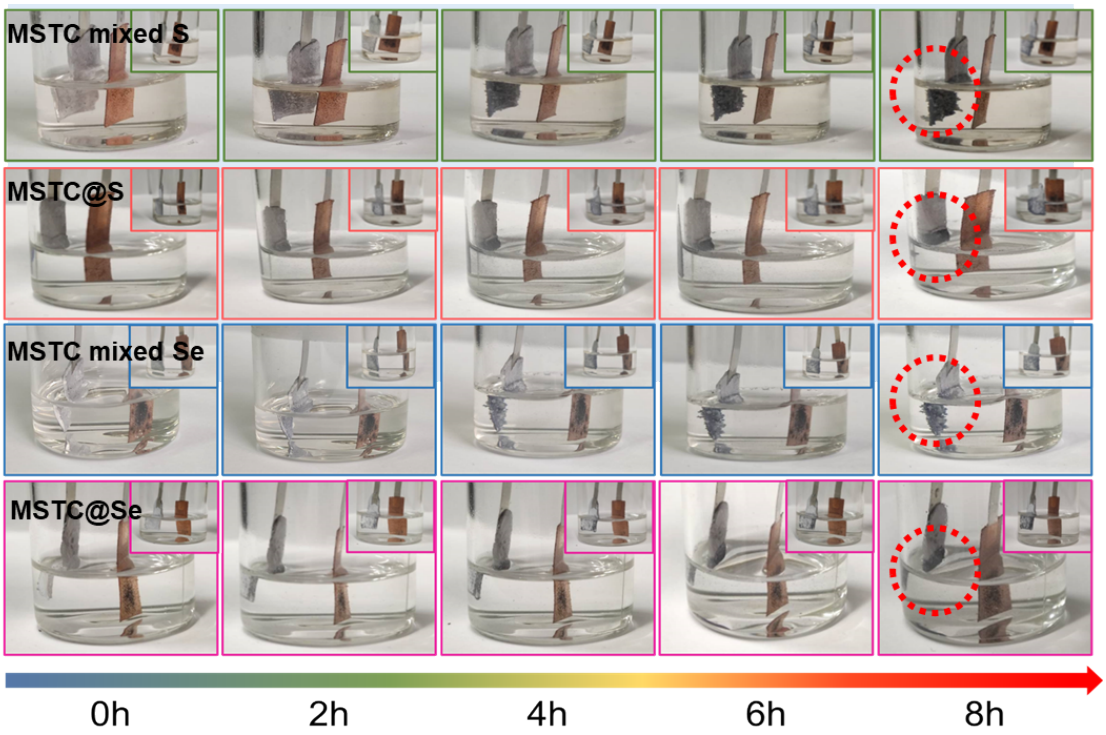

Figure S24. Visual examination of various electrodes test at 2 A g^{-1} for 8 h.

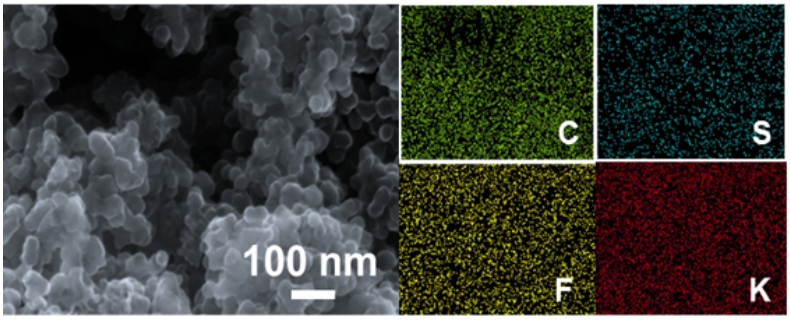

Figure S25. SEM image and the corresponding EDS mapping of MSTC@S after 200 cycles.

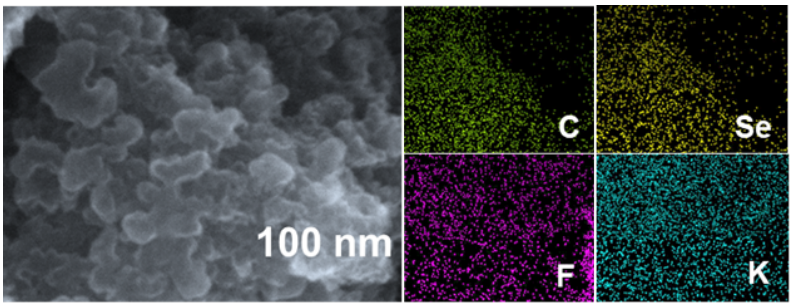

Figure S26. SEM image and the corresponding EDS mapping of MSTC@Se after 200 cycles.

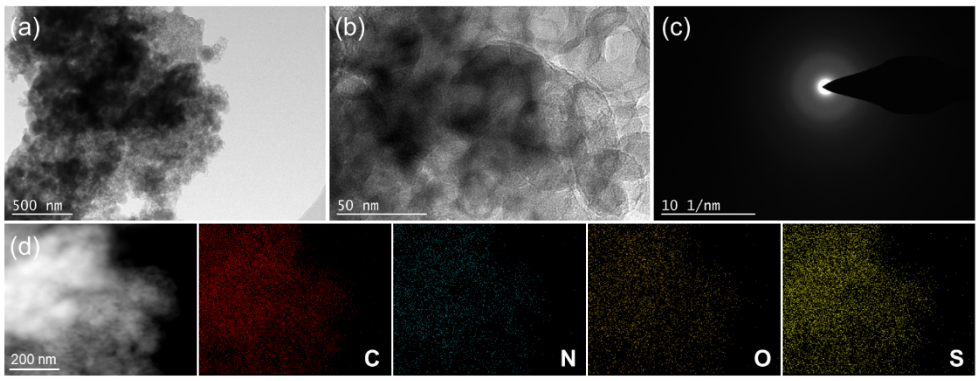

Figure S27. (a, b) TEM images and the corresponding (c) SAED pattern (d) EDS mapping of MSTC@S after cycling.

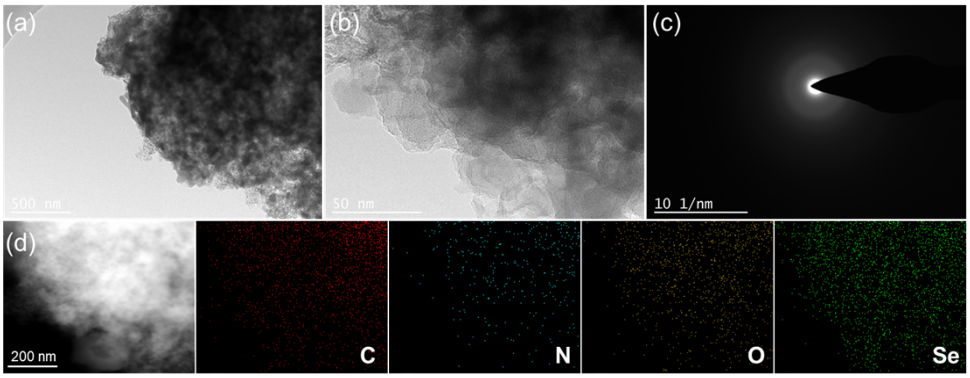

Figure S28. (a, b) TEM images and the corresponding (c) SAED pattern (d) EDS mapping of MSTC@Se after cycling.

Table S1. Physical properties of different samples.

Sample	S_{BET} [a] ($m^2\ g^{-1}$)	V_t [b] ($cm^3\ g^{-1}$)
MSTC	599.8	2.04
MSTC@S	185.4	1.83
MSTC@Se	121.1	0.73

[a] Specific surface area was calculated by the Brunauer-Emmett-Teller (BET) method.

[b] The total pore volume was determined by the density functional theory (DFT) method.

Table S2. Comparisons of the cycling performance of MSTC@Se electrode with other materials in K-Se batteries reported (Note:1C=675 mA g^{-1}).

Sample	Se/wt%	Precursors	Method	Voltage	Electrolyte	Cycling performance	Ref
MSTC@Se	60	Se, carageenan	melt-diffusion	0.5-3.0 V	1.0 M KFSI in EC/DEC	201 mAh g^{-1} (2000 cycles, 2 A g^{-1})	**our work**
Se@NO/CNT	49	Se, ZIF-8	melt-diffusion	0.5-3.0 V	0.7 M KPF_6 in EC/DEC	274 mAh g^{-1} (3500 cycles, 1 A g^{-1})	[2]
Se@NPCFs	62	Se, PAN	molten liquefaction	0.5-3.0 V	0.7 M KPF_6 in EC/DEC	367 mAh g^{-1} (1670 cycles, 0.5 A g^{-1})	[3]
Se@NOPC-CNT	60	Se, chestnut inner shells	impregnation	0.5-3.0 V	0.7 M KPF_6 in EC/DEC	335 mAh g^{-1} (700 cycles, 0.8 A g^{-1})	[4]
Se-O-PCS	51	Se, methyl cellulose	heated	0.5-3.0 V	1.0 M KFSI in EC/DEC	203 mAh g^{-1} (1850 cycles, 1 A g^{-1})	[5]
NSHPC-700/Se	60	Se, glycine	sealed and heated	0.5-3.0 V	1.0 M KFSI in EC/DEC	436 mAh g^{-1} (120 cycles, 0.2 C)	[6]
Se@NPCS	60	Se, ZIF-67	heated	0.5-2.5 V	1.0 M KPF_6 in EC/PC	314 mAh g^{-1} (300 cycles, 0.5 C)	[7]
Se-HPC	42	Se, PANNA	heated	0.5-2.5 V	1.0 M KPF_6 in EC/PC	464 mAh g^{-1} (100 cycles, 0.2 C)	[8]
Se/MDPC	53	Se, ZIF-67	heated	0.7-2.3 V	1.0 M KPF_6 in EC/PC	130 mAh g^{-1} (100 cycles, 0.2 C)	[9]
Se@NMCO	64	Se, PMMA	heated	0.5-3.0V	0.8 M KPF_6 in EC/DEC	148 mAh g^{-1} (1500 cycles, 2 C)	[10]
Se/HHPC	47	Se, PDA	heated	0.5-2.5 V	1.0 M KPF_6 in EC/DEC	236 mAh g^{-1} (300 cycles, 0.2 C)	[11]

Table S3. Comparisons of the cycling performance of MSTC@S electrode with other materials in K-S batteries reported.

Sample	S/wt%	Precursors	Method	Voltage	Electrolyte	Cycling performance	Ref
MSTC@S	60	S, carageenan	melt-diffusion	0.5-3.0 V	1.0 M KFSI in EC/DEC	264 mAh g^{-1} (2000 cycles, 2 A g^{-1})	**our work**
C/S composite	42	S, sucrose	heated	0.5-3.0 V	0.8 M KPF_6 in EC/DEC	870 mAh g^{-1} (150 cycles, 0.02 A g^{-1}) 、	[12]
CCS	39	S, polyacrylonitrile	annealing	0.8-3.0 V	1M KSO_3CF_3 in EC/DEC	253 mAh g^{-1} (300 cycles, 0.15 A g^{-1})	[13]
ACF-1500@S	15	S, ACF	heated	1.2-3.0 V	3.0 M KFSI in DME	157 mAh g^{-1} (250 cycles, 0.05 A g^{-1})	[14]
PCNF/S	25	cyclo-S8, PAN	Sealed and heated	0.5-3.0 V	0.8 M KPF_6 in EC/DEC	1002 mAh g^{-1} (2000 cycles, 0.2 A g^{-1})	[15]
CMK-3/S	41	S, CMK-3	Sealed and heated	1.2-2.4 V	1.0 M $KClO_4$ in TEGDME	202.3 mAh g^{-1} (50 cycles, 0.05 A g^{-1})	[16]
SPAN	38	S, polyacrylonitrile	one-pot method	0.8-2.9V	0.8 M KPF_6 in EC/DEC	147 mAh g^{-1} (100 cycles, 0.12 A g^{-1})	[17]
CCS@CBC-450	40	S, glucose	Sealed and heated	0.01-3.0 V	3 M KTFSI in TEGDME	383 mAh g^{-1} (250 cycles, 0.1 A g^{-1})	[18]
EAMC12	38	S, potassium citrate	Sealed and heated	0.5-3.0 V	0.8 M KPF_6 in EC/DEC	281 mAh g^{-1} (500 cycles, 1.67A g^{-1})	[19]
S@SA-NC	57	S, SA	Sealed and heated	0.5-3.0 V	0.8 M KPF_6 in EC/DEC	371 mAh g^{-1} (200 cycles, 0.84 A g^{-1})	[20]

References

[1] Du, Y.; Fan, H.; Bai, L.; Song, J.; Jin, Y.; Liu, S.; Li, M.; Xie, X.; Liu, W. Molten salt-assisted construction of hollow carbon spheres with outer-order and inner-disorder heterostructure for ultra-stable potassium ion storage. *ACS Applied Materials & Interfaces* 2023, 15 (3), 4081-4091.

[2] Zhou, X.; Wang, L.; Yao, Y.; Jiang, Y.; Xu, R.; Wang, H.; Wu, X.; Yu, Y. Integrating conductivity, captivity, and immobility ability into N/O dual-doped porous carbon nanocage anchored with CNT as an effective Se host for advanced K-Se battery. *Adv. Funct. Mater.* 2020, *30* (43), 2003871.

[3] Xu, R.; Yao, Y.; Wang, H.; Yuan, Y.; Wang, J.; Yang, H.; Jiang, Y.; Shi, P.; Wu, X.; Peng, Z.; et al. Unraveling the nature of excellent potassium storage in small-molecule Se@Peapod-like N-doped carbon nanofibers. *Adv. Mater.* 2020, *32*(52), 2003879.

[4] Yao, Y.; Chen, M.; Xu, R.; Zeng, S.; Yang, H.; Ye, S.; Liu, F.; Wu, X.; Yu, Y. CNT interwoven nitrogen and oxygen dual-doped porous carbon nanosheets as free-standing electrodes for high-performance Na-Se and K-Se flexible batteries. *Adv. Mater.* 2018, *30* (49), e1805234.

[5] Zhou, L.; Cui, Y.; Kong, D.; Feng, W.; Gao, X.; Yan, Y.; Ren, H.; Hu, H.; Xue, Q.; Yan, Z.; et al. Amorphous Se species anchored into enclosed carbon skeleton bridged by chemical bonding toward advanced K-Se batteries. *J. Energy Chem.* 2021, *61*, 319-326.

[6] Kim, J. K.; Kang, Y. C. Encapsulation of Se into hierarchically porous carbon microspheres with optimized pore structure for advanced Na-Se and K-Se batteries. *ACS Nano* 2020, *14* (10), 13203-13216.

[7] Huang, X.; Deng, J.; Qi, Y.; Liu, D.; Wu, Y.; Gao, W.; Zhong, W.; Zhang, F.; Bao, S.; Xu, M. A highly-effective nitrogen-doped porous carbon sponge electrode for advanced K–Se batteries. *Inorg. Chem. Front.* 2020, *7* (5), 1182-1189.

[8] Huang, X.; Wang, W.; Deng, J.; Gao, W.; Liu, D.; Ma, Q.; Xu, M. A Se-hollow porous carbon composite for high-performance rechargeable K–Se batteries. *Inorg. Chem. Front.* 2019, *6* (8), 2118-2125.

[9] Huang, X.; Xu, Q.; Gao, W.; Yang, T.; Zhan, R.; Deng, J.; Guo, B.; Tao, M.; Liu, H.; Xu, M. Rechargeable K-Se batteries based on metal-organic-frameworks-derived porous carbon matrix confined selenium as cathode materials. *J. Colloid Interface Sci.* 2019, *539*, 326-331.

[10] Tian, H.; Liu, H.; Sun, X.; Zhang, C.; Ji, P. Se confined in N-doped mesoporous carbon

opal as anode for K-Se capacitors with super-long cycle life. *JAllC* 2023, *937*, 168376.

[11] Zhao, X.; Wang, D.; Qi, H.; Li, Z.; Yue, H. N/O-doped porous carbon matrix for improved potassium-selenium battery cathode in different electrolyte systems. *Journal of Alloys and Compounds,* 2023, *930*, 167395.

[12] Xiong, P.; Han, X.; Zhao, X.; Bai, P.; Liu, Y.; Sun, J.; Xu, Y. Room-temperature potassium-sulfur batteries enabled by microporous carbon stabilized small-molecule sulfur cathodes. *ACS Nano* 2019, *13* (2), 2536-2543.

[13] Ma, R.; Fan, L.; Wang, J.; Lu, B. Confined and covalent sulfur for stable room temperature potassium-sulfur battery. *Electrochim. Acta* 2019, *293*, 191-198.

[14] Yuan, X.; Zhu, B.; Feng, J.; Wang, C.; Cai, X.; Qin, R. Free-standing, flexible and stable potassium–sulfur battery enabled by controllable porous carbon cloth. *JPS* 2020, *480*.

[15] Zhao, X.; Hong, Y.; Cheng, M.; Wang, S.; Zheng, L.; Wang, J.; Xu, Y. High performance potassium–sulfur batteries and their reaction mechanism. *J. Mater. Chem. A* 2020, *8* (21), 10875-10884.

[16] Zhao, Q.; Hu, Y.; Zhang, K.; Chen, J. Potassium-sulfur batteries: a new member of room-temperature rechargeable metal-sulfur batteries. *Inorg. Chem.* 2014, *53* (17), 9000-9005.

[17] Liu, Y.; Wang, W.; Wang, J.; Zhang, Y.; Zhu, Y.; Chen, Y.; Fu, L.; Wu, Y. Sulfur nanocomposite as a positive electrode material for rechargeable potassium-sulfur batteries. *Chem Commun (Camb)* 2018, *54* (18), 2288-2291.

[18] Bharti, V. K.; Pathak, A. D.; Anjan, A.; Sharma, C. S.; Khandelwal, M. Covalently confined sulfur composite with carbonized bacterial cellulose as an efficient cathode matrix for high-performance potassium–sulfur batteries. *ACS Sustainable Chemistry & Engineering* 2022, *10* (50), 16634-16646.

[19] Hu, L.; Meng, X.; Liu, L.; Liang, D.; Liang, S.; Wang, L. L.; Yang, L.; Ding, T.; Deng, C.; Dong, Q. A superficial sulfur interfacial control strategy for the fabrication of a sulfur/carbon composite for potassium-sulfur batteries. *Chem Commun (Camb)* 2021, *57* (12), 1490-1493.

[20] Ye, C.; Shan, J.; Chao, D.; Liang, P.; Jiao, Y.; Hao, J.; Gu, Q.; Davey, K.; Wang, H.; Qiao, S. Z. Catalytic oxidation of K_2S via atomic Co and pyridinic N synergy in potassium-sulfur batteries. *J. Am. Chem. Soc.* 2021, *143* (41), 16902-16907.